

AD-A250 665

(2)



OFFICE OF NAVAL RESEARCH

GRANT NO. N00014-91-J-1447  
R&T CODE 414044

Technical Report No. 33

BASIC PRINCIPLES OF ORGANOMETALLIC VAPOR PHASE EPITAXY

by

G. B. STRINGFELLOW

**S DTIC  
ELECTED  
MAY 27 1992  
A D**

Prepared for Publication

in the

Proceedings of 8th International School on Crystal Growth

University of Utah  
Dept. of Materials Science & Engineering  
Salt Lake City, UT 84112

May 22, 1992

Reproduction in whole or in part is permitted for any purpose of the  
United States Government

This document has been approved for public release and sale; its  
distribution is unlimited

BASIC PRINCIPLES OF ORGANOMETALLIC VAPOR PHASE EPITAXY  
G.B. Stringfellow  
University of Utah  
Salt Lake City, Utah 84112

ABSTRACT

Crystal growth processes in general and epitaxy in particular are often discussed in terms three disciplines: thermodynamics, mass transport and hydrodynamics, and chemical reaction kinetics. This paper will concentrate on two of these, the thermodynamic and kinetic aspects of organometallic vapor phase epitaxy (OMVPE). Three major influences of thermodynamics will be discussed: 1) Thermodynamics defines the driving force and hence the upper limit of growth rate. This occurs only when all reactants in the system are allowed to equilibrate with the substrate. 2) Thermodynamics often controls stoichiometry and the solid composition of alloys. An understanding of thermodynamic and kinetic constraints leads to the ability to grow metastable alloys. 3) The driving force for phase separation and/or ordering into natural superlattice structures during growth is also governed by thermodynamics. The actual ordered structures observed are dependent on the surface kinetics. This aspect of kinetics will be addressed in addition to the kinetics of both homogeneous and heterogeneous chemical reactions occurring for a variety of precursor molecules. Each of these topics is addressed in terms of fundamental concepts, with examples from recent research on the OMVPE growth of III/V semiconductor compounds and alloys.

1. INTRODUCTION

Epitaxial growth processes, in general, and OMVPE, in particular, are highly complex processes. Indeed, early crystal growth studies were largely empirical, giving crystal growth the appearance of an art. This is partly because of the complex, multicomponent, multiphase systems that are normally of interest and partly because the process is dynamic and inhomogeneous phases are inherent. In an effort to systematically study and understand such a complex system the fundamental processes occurring during epitaxial growth are commonly subdivided into hydrodynamics and mass transport, the kinetics of chemical reactions occurring homogeneously in the gas phase and heterogeneously at the surface, and thermodynamics. We will concentrate on thermodynamics and kinetics in this paper. The hydrodynamic aspects of OMVPE will be addressed in the following paper.

Thermodynamic aspects of epitaxial growth are in many ways the most important. This is especially true when the growth rate is very slow. At low growth rates and relatively high temperatures, the chemical reaction kinetics play less of a role than in very rapid crystal growth processes. In the limit of infinitely slow growth rates thermodynamics defines the concentrations in the vapor and solid phases. Thermodynamics also determines the driving force for any crystal growth process, hence defining the maximum growth rate.

92-13852



Thermodynamics is also used to predict solid composition for many growth conditions. This includes not only alloy composition, but also solid stoichiometry, incorporation of impurities, separation into several solid phases, and the occurrence of ordered superlattice structures in the solid. Thus, the thermodynamic aspects of epitaxy must be understood before proceeding to the kinetic aspects of growth that frequently control growth rate and, in many situations, affect solid composition, the phases appearing, and the occurrence of phase separation and ordering. Increasingly, an understanding of the basic aspects of epitaxy has allowed a departure from the empirical approach to crystal growth.

## 2. THERMODYNAMIC TREATMENT OF OMVPE

The equilibrium state for a two phase,  $\alpha + \beta$ , system is defined in terms of the chemical potentials,

$$\mu_i^\alpha = \mu_i^\beta , \quad (1)$$

where the subscript  $i$  indicates the  $i$ th component and the superscripts indicate the phase. The chemical potential is usually written in terms of the chemical potential in an arbitrary standard state, denoted by the superscript zero,

$$\mu = \mu^o + RT \ln p/p^o. \quad (2)$$

For an ideal gas mixture,

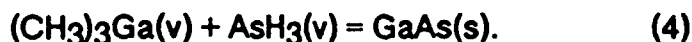
$$\mu_i = \mu_i^0 + RT \ln p_i/p_i^0 , \quad (3)$$

where  $p_i$  is the partial pressure, equal to the mole fraction  $x_i$  multiplied by  $P$ , the total pressure, and the standard state is usually pure component  $i$ .

For an ideal solid solution, the same expression holds with  $p_i/p_i^0$  replaced by  $x_i/x_i^0$ . However, the standard state is pure  $i$ , so  $x_i^0 = 1$ . The form of eq. (3) is so useful that it is retained even for non-ideal solutions with  $x_i$  replaced by the activity,  $a_i$ , which may also be considered a product of  $x_i$  multiplied by a non-ideality factor,  $\gamma_i$ , the activity coefficient.

## 2.1 Driving Force for Epitaxy

For the OMVPE growth of GaAs using trimethylgallium (TMGa) and arsine ( $\text{AsH}_3$ ) the overall reaction is,



Assuming the TMGa and AsH<sub>3</sub> to completely decompose in the gas phase to give Ga and As<sub>4</sub>, an assumption to be revisited in the discussion of kinetics, to follow, the reaction can be simplified:



A-1

2



The equilibrium condition is

$$\mu^v_{\text{Ga}} + 1/4 \mu^v_{\text{As}_4} = \mu^s_{\text{GaAs}}, \quad (6)$$

or

$$\mu^{ov}_{\text{Ga}} + 1/4 \mu^{ov}_{\text{As}_4} + RT \ln p^e_{\text{Ga}} p^{e \frac{1}{4}}_{\text{As}_4} = \mu^{os}_{\text{GaAs}} + RT \ln a_{\text{GaAs}}, \quad (7)$$

where the superscript "e" denotes the equilibrium value of partial pressure. Thus,

$$a_{\text{GaAs}} / p^e_{\text{Ga}} p^{e \frac{1}{4}}_{\text{As}_4} = K_{\text{GaAs}}. \quad (8)$$

where K is the equilibrium constant. This is the basic law of mass action.

When the system is not at equilibrium, the thermodynamic driving force to restore equilibrium is

$$\Delta\mu = \mu^v_{\text{Ga}} + 1/4 \mu^v_{\text{As}_4} - \mu^s_{\text{GaAs}}, \quad (9)$$

or

$$\Delta\mu = RT \ln (p_{\text{Ga}} p_{\text{As}_4}^{\frac{1}{4}} / p^e_{\text{Ga}} p^{e \frac{1}{4}}_{\text{As}_4}). \quad (10)$$

This is the driving force for epitaxy. A situation is intentionally created where higher than equilibrium reactant vapor pressures drive the system to produce the GaAs solid desired. The maximum quantity of GaAs solid that can be produced is simply the amount (the supersaturation) that would establish equilibrium, and is thus fundamentally limited by thermodynamics and the total amount of gas transported through the OMVPE reactor.

For the OMVPE growth of GaAs using arsine and TMGa, the thermodynamic driving force at 100 K is approximately 80 kcal/mol[1]. This is due to the instability of both arsine and TMGa at 1000 K. Thermodynamics also gives a good description of solid composition for the OMVPE growth of III/V and II/VI alloys[2,3].

Ordinarily, in the OMVPE system, the growth rate is considerably less than that calculated from thermodynamics. Kinetics, both surface reaction rates (at low temperatures) and diffusion through the gas phase (at higher temperatures), are not rapid enough to allow equilibrium to be established throughout the system at all times. This situation is illustrated by Fig. 1a, where  $\Delta\mu$  from eq. (9) is plotted versus reaction coordinate. This allows the schematic representation of the overall, thermodynamic driving force for the growth reaction, represented as  $\Delta\mu^*$ . The superscript "\*" denotes the chemical potential in the input gas phase, where for all reactants  $p_i = p^*_i$ . The growth rate is proportional to the flux of atoms diffusing through the boundary layer, which is identical to the flux of atoms crossing the interface into the solid. The diagram shows schematically the driving forces necessary to sustain this flux for the diffusion process ( $\Delta\mu_D$ ) and the surface reactions ( $\Delta\mu_S$ ).

Even in cases with a large supersaturation in the input vapor phase, i.e.,  $\Delta\mu^* >> 0$ , near equilibrium conditions may exist at the growing solid surface. This simply requires that the interface kinetics be much more rapid than the diffusion kinetics, i.e., the two processes proceed at the same rate with  $\Delta\mu_s \ll \Delta\mu_D$ . This situation, termed diffusion limited growth, is shown schematically in Fig. 1b. Using ordinary growth conditions, with temperatures between approximately 550 and 800 C, this is the normal situation for the OMVPE growth of GaAs, as deduced from the nearly temperature independent growth rate, as seen in Fig. 2. For surface kinetically limited processes, the growth rate increases exponentially with increasing temperature[4,5]. This occurs for the OMVPE growth of GaAs at temperatures below approximately 550 C when TMGa is the Ga precursor, but this temperature depends on the group III precursor used, as seen in Fig. 2 and discussed in Section 3, below.

In the diffusion limited case, illustrated schematically in Fig. 1b, the interfacial partial pressures,  $p_i^i$ , nearly satisfy the equilibrium relationship,

$$a_{\text{GaAs}} / p_{\text{Ga}}^i p_{\text{As}_4}^{i/4} = K_{\text{GaAs}} \quad (11)$$

Since the input vapor is highly supersaturated,

$$p^*_{\text{Ga}} p^*_{\text{As}_4}^{1/4} \gg p_{\text{Ga}}^i p_{\text{As}_4}^{i/4} \quad (12)$$

This is equivalent to stating that  $\Delta\mu^* >> 0$ . For the typical case

$$p^*_{\text{Ga}} \ll 4p^*_{\text{As}_4} \quad (13)$$

i.e., the V/III ratio is  $>> 1$ , as will be discussed below. This means that the Ga is nearly depleted at the interface,

$$p_{\text{Ga}}^i \ll p^*_{\text{Ga}} \quad (14)$$

while the As<sub>4</sub> partial pressure is hardly diminished,

$$p_{\text{As}_4}^i \approx p^*_{\text{As}_4} \quad (15)$$

since the same number of As and Ga atoms are removed from the vapor phase to produce GaAs. This situation makes the analysis of growth rate and solid composition particularly simple.

The growth rate is proportional to the flux of Ga and As atoms diffusing through the vapor to the growing interface. For simplicity, this can be analyzed in terms of diffusion through a boundary layer of thickness  $d$ . A more complete description is given in the following paper[6]. The two fluxes are equal, since stoichiometric GaAs is the only product. The flux may be expressed,

$$J = D_{Ga}(p^*_{Ga} - p^i_{Ga})/RTd. \quad (16)$$

where  $D_{Ga}$  is the diffusion coefficient of Ga, in whatever form it may appear while diffusing through the boundary layer. In light of eq. (14), the Ga flux and the GaAs growth rate are proportional to  $p^*_{Ga}$ , as observed experimentally[5]. Equally clear is that the ratio of the concentrations of A and B for alloys with mixing on the group III sublattice,  $A_{1-x}B_xC$ , will be the same as the ratio  $p^*A/p^*B$ , assuming the diffusion coefficients for the A and B species are nearly the same[7,8].

## 2.2 Solution Thermodynamics

The condition for thermodynamic equilibrium is expressed by eq. (1) and the discussion in Section 2.1. Using these concepts, applied to the solid-vapor equilibria of concern for OMVPE, we can calculate the composition of a multicomponent solid alloy from the temperature and the concentrations of the various components in the vapor phase. Deviations from ideality for the vapor phase are commonly neglected. However, non-ideality in the solid phase must be considered. Fortunately, for semiconductor systems the solid can often be described using either the regular solution[9] or "delta-lattice-parameter" (DLP)[10] model. In both cases the distribution of elements on a sublattice is considered to be random, thus the entropy of mixing for a pseudobinary solution of the type  $A_{1-x}B_xC$  is simply the ideal configurational entropy of mixing,

$$\Delta S^M = -R[x \ln x + (1-x) \ln(1-x)]. \quad (17)$$

For the regular solution model, the enthalpy of mixing is obtained by summing nearest-neighbor bond energies, yielding,

$$\Delta H^M = x(1-x) \Omega^S, \quad (18)$$

where  $\Omega^S$  is the interaction parameter. The activity coefficient may be written,

$$\ln \gamma_i = (1-x_i)^2 \Omega / RT. \quad (19)$$

Physically, the regular solution model cannot provide an accurate, predictive description of the enthalpy of mixing in semiconductor alloys. However, simple models developed to interpret the band gap and optical properties can be used to treat the bonding in semiconductor alloys.[10] The DLP model allows accurate calculation of  $\Omega^S$  in terms of the difference in lattice parameters between AC and BC:

$$\Omega^S = 5 \times 10^7 (a_{AC} - a_{BC})^2 [(a_{AC} + a_{BC})/2]^{-4.5}. \quad (20)$$

This first-order treatment of the enthalpy of mixing is apparently equivalent to simply the strain energy caused by the lattice parameter difference[11]. The

solutions are predicted to be ideal for alloys from compounds with the same lattice constant such as GaAs and AlAs, and to have positive deviations from ideality for all other alloys. The DLP model predicts a large positive enthalpy of mixing for systems with a large difference in lattice constant. This can overwhelm the negative configurational entropy of mixing for temperatures below the critical temperature,  $T_c$ , resulting in a free energy versus composition curve with an upward bowing in the center. This dictates that at equilibrium a random alloy in a certain composition range will decompose into a mixture of two phases, i.e., the phase diagram contains a miscibility gap.

The equilibrium conditions for the ternary(or pseudobinary) system may be obtained in exactly the same way as described for binary systems in section 2.1, by equating the chemical potentials of the 2 components in the 2 phases:

$$\mu^V_A + \mu^V_C = \mu^S_{AC} \quad (21a)$$

$$\mu^V_B + \mu^V_C = \mu^S_{BC} \quad (21b)$$

This leads to two mass action expressions, similar to eq. (11). As discussed in section 2.1, equilibrium is assumed to be established at the interface.

As an example of the use of such calculations to understand epitaxial processes, consider the OMVPE growth of  $\text{GaAs}_{1-x}\text{Sb}_x$ . The 2 mass action expressions, one for GaAs and one for GaSb, are solved simultaneously with 2 conservation equations, one for solid stoichiometry and one for solid composition[12]. Complete pyrolysis of the source molecules is normally assumed. This assumption is incorrect for very stable molecules at all temperatures and for all molecules at very low temperatures, as will be discussed below in the Kinetics Section. The activity coefficients of GaAs and GaSb in the solid are calculated as described above using the DLP model.

The calculation can be performed with no adjustable parameters, yielding solid composition versus vapor composition and substrate temperature during growth. The calculated results are compared with experimental data in Fig. 3. Several important aspects of VPE are illustrated in this rather complex figure. First, consider the open data points, obtained for an input V/III ratio (the ratio of the input group V to group III molar flow rates) of 2.0. Notice that the calculated curve for  $V/\text{III} = 2.0$  fits the data well. The Sb distribution coefficient, defined as  $k_{\text{Sb}} = x^S_{\text{Sb}}/x^V_{\text{Sb}}$ , where  $x^V_{\text{Sb}} = p^* \text{TMSb}/(p^* \text{TMSb} + p^* \text{AsH})$ , is seen to be less than unity. GaAs is more stable than GaSb, thus As is more likely to bond to the Ga on the surface and be incorporated into the solid. The excess Sb evaporates from the surface. An additional important point is that the calculation for a V/III ratio of less than unity yields an antimony distribution coefficient of unity. As discussed in Section 2.1 for the case of alloys with mixing on the group III sublattice, when  $V/\text{III} > 1$ , essentially all of the group III elements reaching the interface are incorporated. The case of GaAsSb with mixing on the group V sublattice with  $V/\text{III} \leq 1$  is completely analogous. The establishment of

equilibrium at the interface while the input vapor is highly supersaturated requires that the group V elements be virtually exhausted at the interface. A final point relative to Fig. 3 is the presence of a two solid phase region or miscibility gap. Because of the large difference in lattice constant between GaAs and GaSb a miscibility gap exists[13]. However, when the V/III ratio is less than unity, the As and Sb atoms arriving in a random pattern at the surface do not have time to redistribute themselves into GaAs and GaSb rich areas before being covered over by the next layer. Thus, we are able to grow metastable  $\text{GaAs}_{1-x}\text{Sb}_x$  alloys throughout the entire range of solid composition as shown by the solid data points in Fig. 3. Other, even less stable alloys, such as GaPSb and InPSb can also be grown in this way[14].

## 2.4 Solid Phase Immiscibility

For  $\text{GaAsSb}$ , the value of  $T_c$  is approximately 745 C[12]. At typical growth temperatures, the solid compositions inside the miscibility gap, which covers nearly the entire composition range, cannot be grown by liquid phase epitaxy (LPE)[15]. We have already discussed the ability to grow the metastable alloys by OMVPE. They can also be grown by molecular beam epitaxy (MBE)[16]. Recently, it has been discovered that these alloys may also exhibit an ordered, superlattice structure[17], consisting, in the ideal case, of alternating monolayers of GaAs and GaSb.

Ordering in a thermodynamic system where the random alloy exhibits a large positive enthalpy of mixing is not possible for a regular solution[9], another indication that this model is not physically appropriate for III/V semiconductor alloys. Interestingly, the driving force for ordering is a reduction of strain energy, the same factor that leads to a large positive enthalpy of mixing. The ordered structures are able to accommodate the two dissimilar bond lengths when  $\Delta a \neq 0$  with reduced distortion of the bonds.

Ordering has now been observed in essentially all III/V alloys grown by OMVPE and MBE[11]. The {111} ordered structure (Cu-Pt) with 4 variants, corresponding to the 4 crystallographic distinct {111} planes in a cubic lattice, is normally observed for III/V alloys. Only 2 of the variants are observed during OMVPE growth for (001)-oriented substrates. This is apparently due to the lower symmetry of the reconstructed, As-rich surface. For growth systems where reconstruction is believed absent, such as LPE, no ordering occurs. These and other experimental observations indicate that the ordering phenomena cannot be totally explained by thermodynamic factors: Kinetic factors appear to be important.

## 3. KINETICS

### 3.1 Survey of Precursor Molecules Used for OMVPE

Before discussing the chemical reactions occurring during OMVPE, it is worthwhile to briefly describe the types of precursor molecules used. The

precursors typically contain the desired group III or group V element plus one or more of the radicals H, Cl, CH<sub>3</sub> (methyl), C<sub>2</sub>H<sub>5</sub> (ethyl), C<sub>3</sub>H<sub>7</sub> (propyl), C<sub>4</sub>H<sub>9</sub> (butyl), and others[18]. We have recently entered the period of "designer" precursors, where special precursor molecules are designed for particular applications. Examples are diethylgalliumchloride (DEGaCl) useful for selected area growth[19] and atomic layer epitaxy (ALE)[20], tertiarybutylarsine (TBAs), a less hazardous substitute for arsine,[21] and trimethylamineallane (TMAA), an aluminum source that gives less carbon contamination than the standard trimethylaluminum (TMAI)[22]. The group III hydrides would be very desirable sources for vapor growth since organic radicals frequently result in carbon contamination of the epitaxial layers, as described below. However, the group III hydrides are too unstable. TMAA was designed to resolve this problem by making an adduct compound with trimethylamine to stabilize the alane.

The first requirement of a precursor is that it be sufficiently volatile to allow acceptable epitaxial growth rates. The vapor pressures, along with other properties, are tabulated for group V precursors in Table I. The second requirement is that heating to the desired growth temperature cause pyrolysis. The percent decomposition versus temperature results obtained using an isothermal, flow-tube reactor[23] for several precursors are compared in terms of the values of T<sub>50</sub>, the temperature for 50% pyrolysis under the specific conditions used, in Table I. The relative values of T<sub>50</sub> are often a reflection of the strength of the weakest metal-radical bond in the precursor molecule[18]. Arsine (AsH<sub>3</sub>) and trimethylarsine (TMAs) pyrolyze at the highest temperature since both the H-As and methyl-As bonds are relatively strong. TBAs decomposes at temperatures more than 200°C less than for arsine because of the weak t-butyl-As bond. The nature of the radicals is also the most important factor determining carbon incorporation. Methyl radicals are quite reactive, so frequently lead to carbon incorporation into the growing solid, especially for Al-containing materials[24]. Less reactive radicals, such as t-C<sub>4</sub>H<sub>9</sub>, apparently result in very little carbon contamination. Ethyl radicals are also much less likely than CH<sub>3</sub> to introduce carbon into the solid[25]. Cl doping is apparently not a problem for III/V semiconductors. H radicals actually act to reduce carbon by supplying the H to convert methyl radicals to virtually inert methane[18].

The above discussion of pyrolysis temperature and carbon contamination is somewhat naive, since it implicitly assumes that pyrolysis occurs by homolysis (or heterolysis), i.e., by the sequential elimination of radicals from the parent molecule until the element is incorporated into the solid. For this process, the bond strength determines the pyrolysis temperature and the nature of the resulting radicals largely determines the rate of carbon incorporation into the growing solid. However, the pyrolysis processes may be considerably more complex. As discussed in more detail in the next section, other pyrolysis processes may occur more rapidly than homolysis and produce no reactive radicals.  $\beta$ -elimination reactions[18] occur without radical production, so are favorable for avoiding carbon incorporation, but do not occur for methyl radicals. Pyrolysis of trimethylarsine (TMAs) is believed to occur via hydrogenolysis[26]. In this process, an H<sub>2</sub> molecule interacts directly with the TMAs resulting in the production of CH<sub>4</sub> plus (CH<sub>3</sub>)<sub>2</sub>AsH. The rate of this process is not determined

by the As-CH<sub>3</sub> bond strength and no CH<sub>3</sub> radicals are produced. The ambient can also interact with radicals produced by homolysis to reduce carbon contamination. The highly reactive methyl radicals react with an H<sub>2</sub> ambient to produce methane and reactive, potentially beneficial, H radicals[18].

The major factor driving the initial stages of the search for improved precursor molecules was the demand for less hazardous precursors. Arsine and phosphine are extremely dangerous because of their toxicity combined with their high vapor pressures of many atmospheres. Liquid, organometallic sources are approximately 100X less hazardous solely due to their lower vapor pressures, resulting in slower dispersal into the atmosphere, which, in turn, leads to lower concentrations in case of an accidental release of the precursor into the atmosphere of the laboratory[18]. Fortunately, many organometallic molecules are also considerably less toxic than the hydrides. The outstanding example is tertiarybutylphosphine (TBP), with a toxicity orders of magnitude lower than that for phosphine. Available toxicity data are also included in Table I.

The leading candidates for replacement of the P and As hydrides are TBP and either TBAs or ethylarsine (EAs). All of these molecules yield fairly stable organic radicals during pyrolysis. They also produce MH<sub>2</sub> radicals, where M is either As or P, that act to remove organic radicals from the surface. Thus, carbon contamination appears not to be a problem. In fact, recent data on the growth of GaAs and AlGaAs by OMVPE using TBAs indicates lower carbon concentrations than for growth using arsine[27].

### 3.2 Chemical Reactions

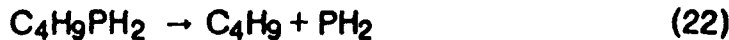
The effects of chemical kinetics are invariably observed during epitaxial growth when the rates of the chemical reactions necessary for growth are slower than the mass transport rates. Thus, the growth rate falls off at low temperatures, as seen in Fig. 2 and discussed above. By comparing the temperature dependence of GaAs growth rates for several Ga precursors, as in Fig. 2, we observe that the pyrolysis of the group III precursor is the rate determining step, not surprising since the V/III ratio is typically much greater than unity. TMGa, with the highest radical-Ga bond strength, gives the lowest growth rate. The Ga-ethyl bond strength is lower, resulting in a higher growth rate for triethylgallium (TEGa). The precursor with the lowest bond strength, triisobutylgallium (TIBGa), gives the highest growth rates at low temperatures. This is an excellent example of the interconnection between the details of pyrolysis of the precursor and growth results. The practical consequence is that efficient low temperature growth can only be accomplished by designing group III precursors with lower bond strengths.

Only recently have the details of the reactions for pyrolysis of the group III and group V precursors, alone and in combination, been studied in detail. The chemical reactions occurring during OMVPE growth often involve complex radical reactions occurring both in the gas phase and on the surface. This is perhaps the most complex and least experimentally accessible aspect of vapor

phase growth. Two approaches have been adopted to study these processes: 1) The study of chemical reactions using analytical techniques such as infrared spectroscopy and mass spectroscopy, either by sampling the exhaust or by in-situ sampling. 2) The study of surface chemical reactions using sophisticated surface analytical techniques that can normally be applied only in UHV chambers. Each approach will be discussed briefly.

Perhaps the simplest approach to studying both homogeneous and heterogeneous chemical reactions involves the use of a mass spectrometer to sample the effluent gas from an ersatz reactor, an isothermal flow-tube reactor[18]. This approach has the advantage of yielding data from which rate constants can be determined. The disadvantage is that intermediate species cannot be detected. Thus, the reaction mechanisms can only be determined by a combination of sophisticated techniques including the use of isotopic labeling of the reactants, the comparison of reaction rates and products in He, H<sub>2</sub>, and D<sub>2</sub> ambients, the addition and removal of radicals from the system, and the use of various times, temperatures, and reactant concentrations. While it can never be claimed that the reaction mechanism has been unequivocally determined, the results and consequent pyrolysis models may be useful guides to the selection of the experimental conditions to be used for OMVPE growth as well as the design of the precursor molecules, themselves.

The only example of this approach considered here will be a brief examination of the pyrolysis of the novel, non-hydride phosphorus precursor TBP. Simply determining the percent decomposition versus temperature for a fixed reaction time but with variable input TBP concentrations reveals that the pyrolysis process is not unimolecular, since the decomposition rate increases with increasing reactant concentration[28]. The products obtained versus reactor temperature for various input concentrations, are shown in Fig. 4. They clearly indicate that several reactions are occurring in parallel, since the product is mainly C<sub>4</sub>H<sub>8</sub> for low input TBP concentrations and C<sub>4</sub>H<sub>10</sub> at higher concentrations. From the product distribution a hypothetical reaction scheme can be suggested, namely that C<sub>4</sub>H<sub>8</sub> is produced by the two sequential unimolecular reactions (22) and (23), below, and that C<sub>4</sub>H<sub>10</sub> is produced by radical attack of the parent molecule, removing an H atom, the 2nd order reaction (28).



The rate of the second order reaction, producing C<sub>4</sub>H<sub>10</sub>, increases more rapidly as the input concentration increases than the rates of the first order reactions (22) and (23). Since a number of other models would give similar results, the hypothetical model has been tested by using[29] deuterated TBPd<sub>2</sub>. The dominant product at high concentrations becomes C<sub>4</sub>H<sub>9</sub>D, supporting the

proposed model. To further test the proposed mechanism, C<sub>4</sub>H<sub>9</sub> radicals were added to the system[30] by adding azo-t-butane (ATB) a compound that pyrolyzes yielding 2 t-butyl radicals and inert N<sub>2</sub> at temperatures below those required for the onset of reaction (22). The temperature for the onset of TBP pyrolysis is dramatically reduced and now coincides with that for ATB. Clearly the t-butyl radicals cause the pyrolysis of TBP. Thus, the indirect evidence, taken together, makes a convincing case that TBP pyrolysis occurs mainly via reactions (22-24). The pyrolysis mechanism for TBAs may be similar, since ATB has been demonstrated to have a similar effect on the pyrolysis rate[30].

Understanding the pyrolysis processes for the individual precursors is directly relevant to understanding and controlling the vapor phase growth techniques. As an example, consider the growth of GaAs and GaP using TMGa plus either TMAs or TBP. The results of systematic studies of the interactions between TMGa and TBP indicate that the PH<sub>2</sub> radicals generated during TBP pyrolysis [reaction (22)] attack TMGa on the semiconductor surface, enhancing their pyrolysis rate by removing CH<sub>3</sub> radicals[29,31]. This is also an important process for removing methyl radicals from the system, resulting in a reduction in carbon contamination. Recent results for GaAs grown using TMGa demonstrate TBAs pyrolysis probably also generates AsH<sub>2</sub> radicals.

The chemical reactions occurring specifically at the semiconductor surface have been studied fairly intensively by using UHV surface spectroscopic probes developed for the study of catalysis, such as electron diffraction, photoemission, Auger electron spectroscopy, electron energy loss spectroscopy, thermally programmed desorption, and modulated beam mass spectroscopy (MBMS)[32,33]. The elementary processes involved in UHV growth techniques, chemical beam epitaxy(CBE) for example, such as the heterogeneous pyrolysis of TEGa, have been the subject of dozens of studies within the last few years. Such studies have the advantage of simplicity. Thus, they may give more direct, less ambiguous information about chemical reactions than the more complex experiments described above for combined group III and group V precursors in a flowing, atmospheric-pressure ambient. Nevertheless, the experimental conditions are frequently very dissimilar to those used for growth, even under UHV conditions where gas phase collisions do not occur. The times involved are frequently very different than those important for growth processes. In addition, the species on the surface may interact during growth. Thus, having a specific surface coverage of a single species, although convenient experimentally, may reveal little about the actual processes occurring during epitaxial growth where the surface coverage may be much different. The most meaningful experiments are probably those involving the simultaneous presence of both group III precursors, such as TEGa, TMGa, or trimethylindium (TMI<sub>n</sub>), and group V molecules, such as As dimers and/or tetramers.

Using these surface probes, the complex dependence of growth rate on temperature for TEGa combined with As<sub>2</sub> has been carefully studied and modeled. Martin and Whitehouse[32] have devised the following scheme based on their MBMS studies. As expected, at very low temperatures, TEGa does not

pyrolyze. At temperatures up to 350°C, DEGa is formed, but desorbs without further decomposition. Thus, the growth rate remains nearly zero. As the temperature is increased above 350°C, the growth rate increases, since the pyrolysis can now proceed to elemental Ga. However, a progressive decrease in growth rate is observed as the temperature is raised above approximately 440°C, due to an increasing rate of desorption of DEGa. This competes with the growth process. Interestingly, the basic scheme agrees with the earlier suggestions of Robertson et al[34], based on a simple, intuitive model. Perhaps more importantly, these surface spectroscopy experiments give information useful in understanding more complex problems, such as the rather complex effects of temperature and group III fluxes on the composition of alloys, i.e., GaInAs and AlGaAs[32]. This type of information is also expected to be extremely valuable in the design of new group III precursors for CBE.

### 3.3. Motion of Surface Steps

Surface analytical techniques that can be applied during MBE growth (but not for OMVPE, because of the electron-absorbing atmosphere) have given considerable information about the atomic configurations on semiconductor surfaces under various conditions. The unreconstructed As-rich (001) GaAs surface consists of As atoms forming only two bonds to underlying Ga atoms. The two dangling bonds per surface atom give this configuration a very high energy. The energy is reduced dramatically by the formation of dimers between adjacent As atoms[35]. These dimers run in [110] rows on the surface. An atom being attached to a kink moving along the step, the process leading to growth, thus sees two types of sites[36]. One involves the formation of bonds to the underlying lattice atoms and the other also involves the formation of a dimer bond. In addition, the location of the dimers is correlated to the size of the underlying atoms. These two factors give rise to the formation of 2 particular variants of the Cu-Pt structure during growth on (001)-oriented substrates[11,36]. The model correctly predicts the formation of the same two variants for both alloys with mixing on the group III sublattice, such as GaInP, and for those with mixing on the Group V sublattice, such as GaAsP[36]. The model also predicts that the direction of [110] step motion will determine which of the two variants will be formed. This is dramatically confirmed by recent experiments where the direction of step motion has been controlled by patterning the surface with [110]-oriented grooves[37,38]. The GaInP grown on the two sides of the groove is produced by the motion of steps in opposite directions[37]. This results in each half of the groove being filled by a single domain, consisting entirely of a material ordered with the same variant of the Cu-Pt structure. Similar, but slightly more complex, results have been obtained for GaAsP[38]. This is a dramatic demonstration of the control of ordering. These are the first macroscopic ordered domains ever produced in III/V alloys. The cross sectional size is 1/2 the groove width by the layer thickness. The length is the dimension of the substrate, i.e., the length of the groove.

## 4. SUMMARY

Thermodynamics acts as the driving force for epitaxial growth and thus places an upper limit on the OMVPE growth rate. If all of the nutrient phase in the reactor were able to equilibrate with the solid epitaxial layer being grown, the system would be operating at the maximum possible growth rate. This is virtually never the case because of mass transport and surface kinetic limitations. For "normal" growth rates and temperatures the chemical reaction kinetics are considerably more rapid than diffusion. Thus, most of the vapor phase supersaturation is used to drive the diffusion process. As a result, the vapor phase adjacent to the growing interface is nearly in equilibrium with the solid. This situation allows the construction of a simple model that can be used to accurately predict the solid compositions in III/V alloys in terms of the input vapor pressures and substrate temperature during growth.

Miscibility gaps exist in many III/V alloys due to the large difference in lattice parameters between the binary end components. OMVPE has been used for the growth of metastable alloys. The key to growing these metastable alloys is the input V/III ratio. When  $V/III < 1$ , all of the As and Sb reaching the interface are incorporated. The random As and Sb distribution expected from the random impingement from the vapor phase might be expected to result in a nearly random alloy. However, ordered structures are commonly observed in electron diffraction patterns. The ordering is due to the high strain energy inherent in a random solid alloy consisting of bonds with different preferred lengths. The formation of ordered structures reduces this microscopic strain energy.

The kinetic aspects of epitaxy are by far the most complex and, consequently, the least understood. We are beginning to understand the reactions involved in the homogeneous and heterogeneous pyrolysis of the wide variety of group III and group V precursors used for OMVPE. These reactions are often complex, involving second order processes such as the attack of the parent molecules by free radicals produced during homolysis. The processes occurring on the surface that lead to growth are even more complex. Both simple bond breaking to produce radicals and radical attack reactions apparently occur heterogeneously. In addition, desorption of parent molecules and intermediates controls the growth rate under certain conditions, as convincingly demonstrated for the CBE growth of GaAs from TEGa and cracked arsine. The physical processes, such as surface reconstruction and step motion, also have profound effects on the solid formed, including the occurrence of phase separation and ordering.

#### ACKNOWLEDGMENTS

The author gratefully acknowledges the financial support of the Department of Energy, the Office of Naval Research, and the Airforce Office of Scientific Research.

**Table I:** Properties of group V sources used for epitaxy. The values of vapor pressure and toxicity were obtained from ref. 18, unless otherwise indicated. The values of pyrolysis temperature ( $T_{50}$ ) were obtained from similar experiments in an atmospheric-pressure, flow-tube reactor with a residence time of a few seconds.

Precursor	Vapor Pressure p.Torr/T. $^{\circ}$ C	$T_{50}$ ( $^{\circ}$ C)	Toxicity LC50** (TLV*)	Carbon Doping TMGa/TMIn
PH <sub>3</sub>		850	11-50 (0.3)	Very Low
TBP	141/10	450	>1100	Low
AsH <sub>3</sub>		600	5-50 (0.05)	Very Low
TMA <sub>s</sub>	238/20	530	20,000	Very High
TEAs	5/20	490	500-1000***	High
DMA <sub>s</sub>	176/0	460	130	High
DEAs	40/20	440	300	Low
EAs	145/-7 <sup>a</sup>	440		Low
TBAs	96/10	380	70	Very Low
PhAsH <sub>2</sub>	1.8/20 <sup>b</sup>			High
(C <sub>6</sub> H <sub>5</sub> )AsH <sub>2</sub>				

\* TLV based on average eight hour work day

\*\* Based on study of rat mortality after 4 hour exposure

\*\*\*Oral dose in mg of material per kg of animal weight.

a) D.M. Speckman and J.P. Wendt, *J. Crystal Growth* 105, 275 (1990).

b) A. Brauers, O. Kayser, R. Kall, H. Heinecke, P. Balk, and H. Hofmann, *J. Crystal Growth* 93, 7 (1988).

## FIGURE CAPTIONS

Figure 1. Schematic diagram of chemical potential versus reaction coordinate, showing the drop in chemical potential required for each step in the growth sequence to keep all rates equal. The differences in individual chemical potentials can alternatively be thought of as ratios of partial pressures of the reactants: a) the general case (After Stringfellow[39]) and b) the case of rapid surface kinetics, i.e., with  $\Delta\mu_s \ll \Delta\mu_D$  (After Stringfellow [40]).

Figure 2. Growth efficiency (growth rate/group III molar flow rate) versus reciprocal temperature for various Ga alkyls: TMGa (■), TEGa (●), and TIBGa (▲). (After Stringfellow[41]). The data are from Plass et al[42].

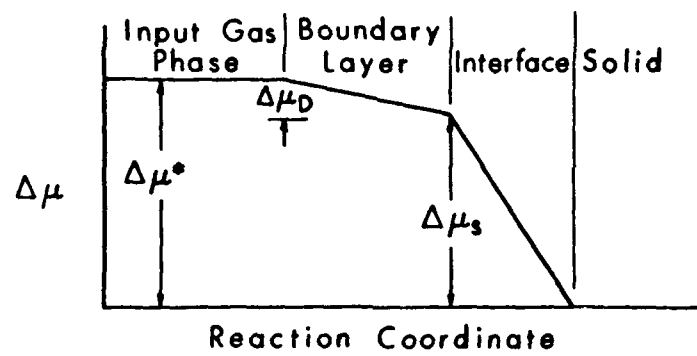
Figure 3. Solid versus vapor composition for the alloy  $\text{GaAs}_{1-x}\text{Sb}_x$ . The data are from the work of Cooper et al[43] for V/III = 2.0(○), and V/III = 0.5(◐), and the work of Stringfellow and Cherng[44](●). The curves were calculated for various V/III ratios. The broken sections of each curve represent the calculated regions of solid immiscibility. (After Stringfellow and Cherng[44]).

Figure 4. Products of TBP decomposition versus temperature for several initial TBP concentrations. (After Li et al[45]).

## REFERENCES

- 1) G.B. Stringfellow J. Crystal Growth **115** 1 (1992).
- 2) G.B. Stringfellow, *Organometallic Vapor Phase Epitaxy: Theory and Practice*, (Academic Press, Boston, 1989), Chapter 3.
- 3) D.W. Kisker and A.G. Zawadski, J. Crystal Growth **89**, 378 (1988).
- 4) D. W. Shaw, *Treatise on Solid State Chemistry*, Vol 5, ed., N.B. Hannay (Plenum, New York, 1975) p. 283.
- 5) See Ref. 2, Chapter 1.
- 6) K. F. Jensen, "MOCVD Growth, Flow Dynamics, and Reactor Design", Presented at the Eight International Summer School on Crystal Growth, August 9-15, 1992, Palm Springs, California.
- 7) G. B. Stringfellow, *Crystal Growth of Electronic Materials*, ed. E. Kaldis (Elsevier Science Publishers B.V., Amsterdam, 1985) p. 247.
- 8) G. B. Stringfellow, *Semiconductors and Semimetals*, Vol 22, Part A, ed. W. T. Tsang (Academic Press, Inc, Orlando, 1985), p. 209.
- 9) R. A. Swalin, *Thermodynamics of Solids* (John Wiley and Sons, New York, 1962).
- 10) G. B. Stringfellow, J. Crystal Growth **27** 21 (1974).
- 11) G.B. Stringfellow, J. Crystal Growth **98**, 108 (1989).
- 12) G. B. Stringfellow, J. Crystal Growth **62** 225 (1983).
- 13) M.J. Cherng, R.M. Cohen and G.B. Stringfellow, J. Electron. Mater. **13**, 799 (1984).
- 14) M.J. Jou and G.B. Stringfellow, J. Crystal Growth **98**, 679 (1989).
- 15) J. R. Pessetto and G. B. Stringfellow, J. Crystal Growth **62** 1 (1983).
- 16) J. Waho, S. Ogawa and S. Maruyama, Japan. J. Appl. Phys. **16** 1875 (1977).
- 17) H. R. Jen, M. J. Cherng, and G. B. Stringfellow, Applied Physics Letters **48**, 1603 (1986).
- 18) Reference 2, Chapter 2.
- 19) T.F. Kuech, M.S. Goorsky, M.A. Tischler, A. Palevski, P. Solomon, R. Potemski, C.S. Tsai, J.A. Levens, and K.J. Vahala, J. Crystal Growth **107**, 116 (1991).
- 20) K. Mori, M. Yoshida, A. Usui, and H. Terao, Appl. Phys. Lett. **52**, 27 (1988).
- 21) C.H. Chen, C.A. Larsen, and G.B. Stringfellow, Appl. Phys. Lett. **50**, 218 (1987); R.M. Lum, J.K. Klingert, and M.G. Lamont, Appl. Phys. Lett. **50**, 284 (1987).
- 22) A.C. Jones and S.A. Ruchworth, J. Crystal Growth **107**, 350 (1991).
- 23) N.I. Buchan, C.A. Larsen, and G.B. Stringfellow, Appl. Phys. Lett. **51**, 1024 (1987).
- 24) T.F. Kuech, D.J. Wolford, E. Veuhoff, V. Deline, P.M. Mooney, R. Potemski, and J. Bradley, J. Appl. Phys. **62**, 632 (1987).
- 25) R. Bhat , P. O'Connor, H. Tempkin, R. Dingle, and V.G. Keramidas, Inst. Phys. Conf. Ser. **63**, 101 (1982).
- 26) S.H. Li, C.A. Larsen, and G.B. Stringfellow, J. Crystal Growth **102**, 117 (1990).
- 27) S.P. Watkins and G. Haacke, Appl. Phys. Lett. **59**, 2263 (1991).
- 28) S.H. Li, C.A. Larsen, N.I. Buchan, and G.B. Stringfellow, J. Electron. Mater. **18**, 457 (1989).

- 29) S.H. Li, C.A. Larsen, N.I. Buchan, G.B. Stringfellow, W.P. Kosar, and D.W. Brown, *J. Appl. Phys.* **65**, 5161 (1989).
- 30) S.H. Li, C.A. Larsen, N.I. Buchan, and G.B. Stringfellow, *J. Crystal Growth* **98**, 309 (1989).
- 31) S.H. Li, N.I. Buchan, C.A. Larsen, and G.B. Stringfellow, *J. Crystal Growth* **96**, 906 (1989).
- 32) T. Martin and C.R. Whitehouse, *J. Crystal Growth* **105**, 57 (1990).
- 33) E.M. Gibson, C.T. Foxon, J. Zhang, and B.A. Joyce *J. Crystal Growth* **105**, 81 (1990).
- 34) A. Robertson, T.H. Chiu, W.T. Tsang, and J.E. Cunningham, *J. Appl. Phys.* **64**, 877 (1988).
- 35) D.J. Chadi, *J. Vac. Sci. and Technol.* **A5**, 834 (1987).
- 36) G.S. Chen, D.S. Jaw, and G.B. Stringfellow, *J. Appl. Phys.* **69**, 4263 (1991).
- 37) G.S. Chen and G.B. Stringfellow, *Appl. Phys. Lett.* **59**, 324 (1991).
- 38) G.S. Chen and G.B. Stringfellow, *Appl. Phys. Lett.* **59**, 3258 (1991).
- 39) G.B. Stringfellow *J. Crystal Growth* **68**, 111 (1984).
- 40) G.B. Stringfellow *J. Crystal Growth* **70**, 133 (1984).
- 41) See reference 2, Chapter 6.
- 42) C. Plass, H. Heinecke, O. Kayser, H. Luth, and P. Balk, *J. Crystal Growth* **88**, 455 (1988).
- 43) C.B. Cooper, R.R. Saxena, and M.J. Ludowise, *J. Electron. Mater.* **11** 1001 (1982).
- 44) G.B. Stringfellow and M.J. Cherng, *J. Crystal Growth* **64** 413 (1983).
- 45) S.H. Li, C.A. Larsen, N.I. Buchan, and G.B. Stringfellow, *J. Electron. Mater.* **18**, 457 (1989).



(a)

